# Numerical Investigation of the Influence of Viscoelasticity on Drop Deformation in Shear

K. Verhulst*, R. Cardinaels*, P. Moldenaers*, Y. Renardy† and S. Afkhami†

*Katholieke Universiteit Leuven, Department of Chemical Engineering, W. de Croylaan 46 - B 3001 Heverlee (Leuven), Belgium
†Dept. of Mathematics and ICAM, 460 McBryde Hall, Virginia Tech, Blackburg VA 24061-0123, USA

**Abstract.** Numerical simulations and experimental data are compared for the investigation of the influence of viscoelasticity on drop deformation in shear. A viscoelastic drop suspended in a Newtonian liquid, or a Newtonian drop suspended in a viscoelastic liquid, is sheared and investigated for transients, relaxation after cessation of shear flow, and step-up in shear rate. The numerical simulations are conducted at parameters chosen to model the experiments. We use the volume of fluid (VOF) continuum surface force (CSF) algorithm for situations dominated by shear. For drop relaxation experiments, we use the paraboloid representation of the interface in the surface tension force (PROST) algorithm. The Oldroyd-B and Giesekus constitutive models are implemented. An interesting result is that by stepping up in the capillary number gradually, a stationary states is achieved at higher capillary numbers than without the graduated steps. The experimental work is described in Verhulst, Moldenaers and Cardinaels [1]. We present a summary of the numerical approach here. The reader is referred to [2] for details.

**Keywords:** drop deformation, Oldroyd-B model, volume-of-fluid method, blend morphology, viscoelasticity
**PACS:** 47.11.-j, 47.55.D-, 47.50.Ef

## INTRODUCTION

The influence of matrix and droplet viscoelasticity on drop deformation and relaxation under shear is investigated for the blend systems described in [1]. The viscoelastic liquids are constant viscosity Boger fluids, which are described by the Oldroyd-B constitutive model. Experimental data are described in [3, 4].

For each liquid, the solvent viscosity is denoted $\eta_s$, polymeric viscosity $\eta_p$, total viscosity $\eta = \eta_s + \eta_p$, relaxation time $\tau$, density $\rho$, and the shear rate is $\dot{\gamma}$. Additional subscripts 'd' and 'm' denote the drop and matrix liquids. The governing equations include incompressibility and momentum transport:

$$\nabla \cdot \mathbf{u} = 0, \qquad \rho\left(\frac{\partial \mathbf{u}}{\partial t} + \mathbf{u} \cdot \nabla \mathbf{u}\right) = \nabla \cdot \mathbf{T} - \nabla p + \nabla \cdot \left(\eta_s(\nabla \mathbf{u} + (\nabla \mathbf{u})^T)\right) + \mathbf{F}, \tag{1}$$

where $\mathbf{T}$ denotes the extra stress tensor. The total stress tensor is $\underline{\tau} = -p\mathbf{I} + \mathbf{T} + \eta_s[\nabla \mathbf{u} + (\nabla \mathbf{u})^T]$. Each liquid is identified with a color function,

$$C(\mathbf{x},t) = \begin{cases} 0 & \text{in the matrix liquid} \\ 1 & \text{in the drop} \end{cases} \tag{2}$$

which advects with the flow. The position of the interface is approximated by the location of the discontinuity in $C(\mathbf{x},t)$. The interfacial tension force is formulated as a body force $\mathbf{F} = \Gamma \tilde{\kappa} \mathbf{n} \delta_S$, $\tilde{\kappa} = -\nabla \cdot \mathbf{n}$, where $\Gamma$ denotes the surface tension coefficient, $\mathbf{n}$ the normal to the interface, $\delta_S$ the delta-function at the interface, and $\tilde{\kappa}$ the curvature. Here, $\mathbf{n} = \nabla C/|\nabla C|$, $\delta_S = |\nabla C|$. We implement the Giesekus constitutive equation for the drop and matrix liquids:

$$\tau\left(\frac{\partial \mathbf{T}}{\partial t} + (\mathbf{u} \cdot \nabla)\mathbf{T} - (\nabla \mathbf{u})\mathbf{T} - \mathbf{T}(\nabla \mathbf{u})^T\right) + \mathbf{T} + \tau\kappa\mathbf{T}^2 = \eta_p(\nabla \mathbf{u} + (\nabla \mathbf{u})^T). \tag{3}$$

In one limit, this reduces to the Oldroyd-B model. The viscoelastic liquids used in the experiments are, as a first approximation, Oldroyd-B liquids [4]. The dimensionless parameters are the viscosity ratio (based on total viscosities) $\lambda = \frac{\eta_d}{\eta_m}$, a capillary number $Ca = \frac{R_0 \dot{\gamma} \eta_m}{\Gamma}$, a Weissenberg number per fluid $We = \dot{\gamma}\tau$, and retardation parameter per fluid $\beta = \frac{\eta_s}{\eta}$. Here, $R_0$ denotes the initial radius of the drop. A Reynolds number based on the matrix liquid $Re = \frac{\rho \dot{\gamma} R_0^2}{\eta_m}$ is in the range .01 to .05, chosen small so that inertia is negligible. Alternatively, let $\Psi_1$ denote the first normal stress coefficient, equivalent to $2\eta_p\tau$, and define the Deborah number by $\widetilde{De} = \frac{\Psi_1 \Gamma}{2R_0\eta^2}$; i.e., $\widetilde{De}_d = (1-\beta_d)We/(\lambda Ca)$, and

CP1027, *The XV^th International Congress on Rheology, The Society of Rheology 80^th Annual Meeting*
edited by A. Co, L. G. Leal, R. H. Colby and A. J. Giacomin

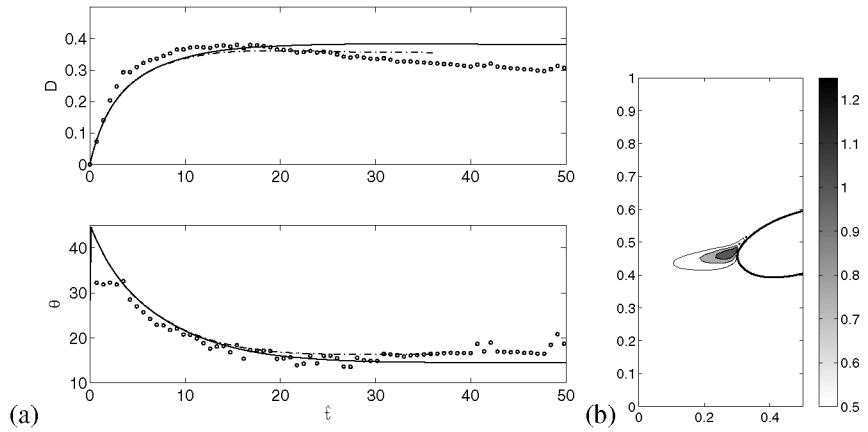


**FIGURE 1.** Newtonian drop in Boger fluid matrix with $Ca = 0.35$, $\widetilde{De}_m = 1.89$, $\lambda = 1.5$, $\beta_m = 0.68$. (a) Evolution of side-view $D$ and $\theta$ *vs.* $\hat{t}$. Experimental data o; 3D Oldroyd-B model —; Giesekus model with $\hat{\kappa}_m = 0.01$ $-\cdot$. (b) Viscoelastic stress contour plot in the x-z plane for $\widetilde{De}_m = 1, \hat{t} = 40$.

$\widetilde{De}_m = (1-\beta_m)We/Ca$. Results are presented below in terms of the Deborah numbers, and dimensionless capillary time $\hat{t} = \frac{t\Gamma}{\eta_m R_0} = \frac{t\dot{\gamma}}{Ca}$. The rescaled Giesekus parameter is $\hat{\kappa} = \kappa\eta_p$. Its physically viable range is $0 \leq \hat{\kappa} < 0.5$

The numerical algorithm is the volume-of-fluid (VOF) method given in Ref. [5]. The interfacial tension force is approximated by either the continuum surface force formulation (CSF) or the parabolic representation of the interface for the surface tension force (PROST). The reader is referred to [6, 2, 7] for these algorithms. Both VOF-PROST and VOF-CSF codes are parallelized with OpenMP [8].

The computational domain is denoted $0 \leq x \leq L_x, 0 \leq y \leq L_y, 0 \leq z \leq L_z$. The walls at $z = 0, L_z$ move with speeds $\pm U_0$, driving a velocity field $(U(z),0,0)$ in the absence of the drop, where $U(z) = U_0(2z - L_z)/L_z$. The shear rate is $\dot{\gamma} = U'(z) = 2U_0/L_z$. Spatial periodicity is imposed in the $x$ and $y$ directions, at $x = 0, L_x$ and $y = 0, L_y$, respectively. $L_x, L_y$ and $L_z$ are chosen to minimize the effect of neighboring drops and that of the walls. Typically, the distance between the walls is eight times the drop radius, as is the spanwise period, and the period in the flow direction is chosen dependent on drop extension.

Initially, the drop is spherical, and the walls are impulsively set into motion. This requires that the viscoelastic stress tensor and velocity are initially zero.

The same notation as in [4, 9] is used for drop diagnostics: the cross-section in the $x-z$ plane, or the velocity-velocity gradient plane, provides the drop length $L$ and breadth $B$. The angle of inclination to the flow direction is denoted $\theta$. Deformation is defined by $D = (L-B)/(L+B)$.

## RESULTS

In the case of a Boger fluid matrix, viscoelastic stress fields, computed at varying $\widetilde{De}_m$, show maxima slightly above the drop tip at the back and below the tip at the front. The area of largest viscoelastic stress moves from the drop tip slightly upwards during drop evolution. The Oldroyd-B model is confirmed to predict the experimental data. Matrix viscoelasticity significantly suppresses droplet deformation and promotes droplet orientation. These effects saturate at high $\widetilde{De}_m$ at fixed $Ca$, as in the 2D simulations of [10]. The location of the maxima for viscoelastic stress is slightly above the drop tip at the back of the drop rather than at the drop tips, directly at the interface. This is a narrow region, and appears to correspond with the dividing streamline. Figure 1 shows evolution for $Ca = 0.35$, $\widetilde{De}_m = 1.89$, $\beta_m = 0.68$, $\lambda = 1.5$; experimental data (o) vs 3D Oldroyd B model (—) and the Giesekus model with $\hat{\kappa}_m = 0.01$. There is a slight overshoot in deformation in the Oldroyd B simulation, after which it settles to a constant $D$ and $\theta$. The Giesekus model displays slightly more damping. The data shows additional damping for large $t$, which may reflect the presence of more than one relaxation time.

The influence of droplet viscoelasticity on deformation is weak, as seen in the droplet shape after inception or cessation of shear, even at high $Ca$ and $\widetilde{De}_d$. Figure 2 is a comparison of simulations and data [4]. At $Ca = 0.14$, the result is similar to the Newtonian case. For $Ca = 0.32$, deformation is less than the Newtonian case. For fixed

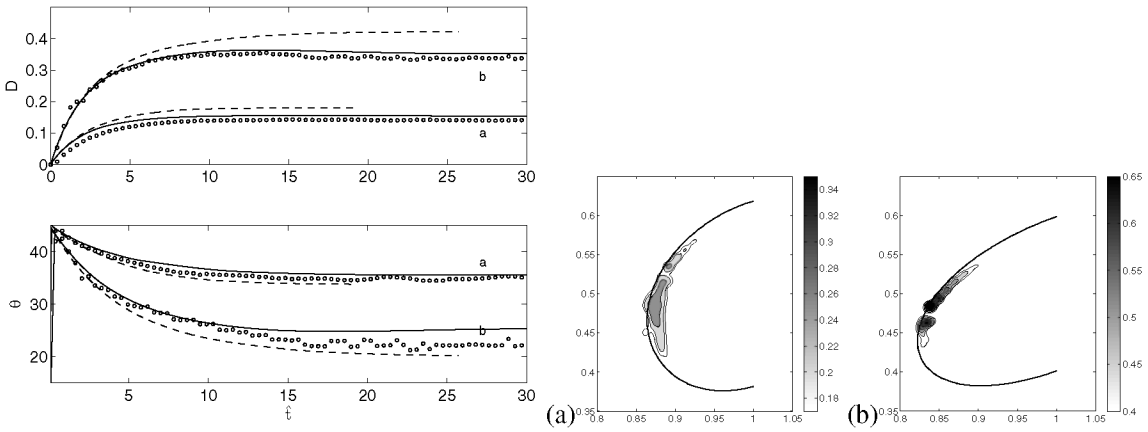


**FIGURE 2.** Side view deformation, 3D VOF-CSF simulation (—) and experimental data ($o$) at fixed $\widetilde{De}_d = 1.54$, $\beta_d = 0.68$, for varying $Ca =$ (a) 0.14; (b) 0.32, and Newtonian CSF simulation ($--$). The contours for viscoelastic stresses at stationary states are given.

Deborah number, the magnitude of viscoelastic stress increases with capillary number. The location of the maximum viscoelastic stress migrates to slightly above the drop tip at the back, and slightly below the drop tip at the front when stationary state is reached.

## ACKNOWLEDGMENTS

This research is supported by NSF-DMS-0456086, NCSA CTS060022, GOA 03/06 and FWO-Vlaanderen (fellowship for R. Cardinaels). We thank Prof. T. Sridhar (Monash University) for measuring the extensional rheology of our samples, and P. Gillioen and Dr J. Lauger (Anton Paar) for help with the counter-rotating device.

## REFERENCES

1. K. Verhulst, R. Cardinaels, P. Moldenaers, Y. Renardy, and S. Afkhami, "Steady state droplet deformation and orientation during bulk and confined shear flow in blends with one viscoelastic component: Experiments, modeling and simulations," in *Proc.XVth International Congress on Rheology*, American Institute of Physics, 2008.
2. Y. Renardy, and M. Renardy, *J. Comp. Phys.* **183**, 400–421 (2002).
3. K. Verhulst, P. Moldenaers, and M. Minale, *J. Rheol.* **51**, 261–273 (2007).
4. K. Verhulst, R. Cardinaels, P. Moldenaers, Y. Renardy, and S. Afkhami, *Submitted to J. Non-Newtonian Fluid Mech* (2007).
5. D. Khismatullin, Y. Renardy, and M. Renardy, *J. Non-Newtonian Fluid Mech.* **140**, 120–131 (2006).
6. J. Li, Y. Renardy, and M. Renardy, *Phys. Fluids* **12**, 269–282 (2000).
7. T. Chinyoka, Y. Renardy, M. Renardy, and D. B. Khismatullin, *J. Non-Newtonian Fluid Mech.* **130**, 45–56 (2005).
8. Y. Renardy, and J. Li, *SIAM News* **33(10)**, 1 (2000).
9. A. Vananroye, P. V. Puyvelde, and P. Moldenaers, *J. Rheol.* **51(1)**, 139–153 (2007).
10. P. Yue, J. J. Feng, C. Liu, and J. Shen, *J. Fluid Mech.* **540**, 427–437 (2005).